The Low Frequency Array (LOFAR): The EoR project

Saleem Zaroubi, on behalf of the LOFAR EoR team

The History

Credit: Science magazine

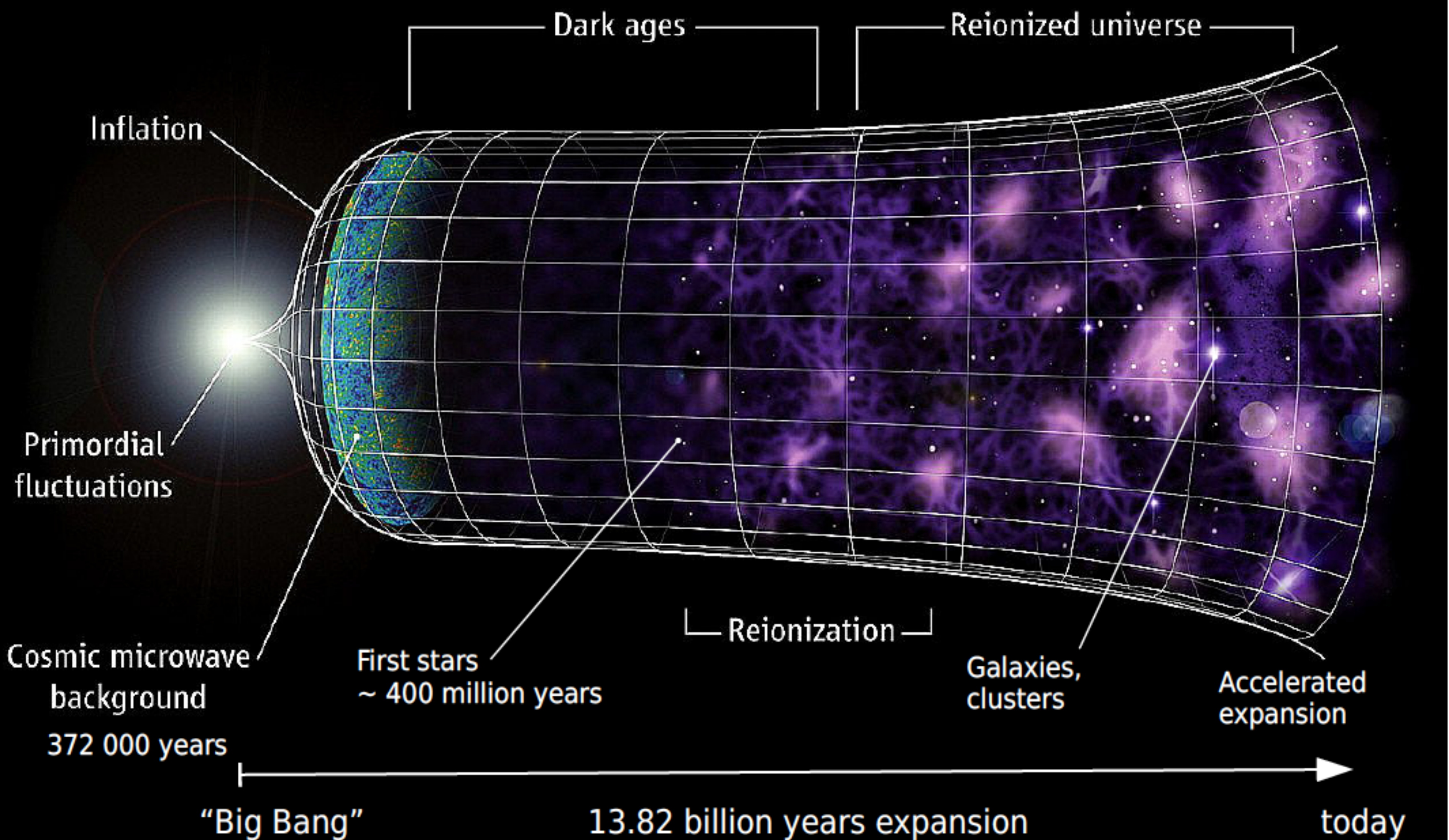

Credit: M. Alvarez

The 21 cm line

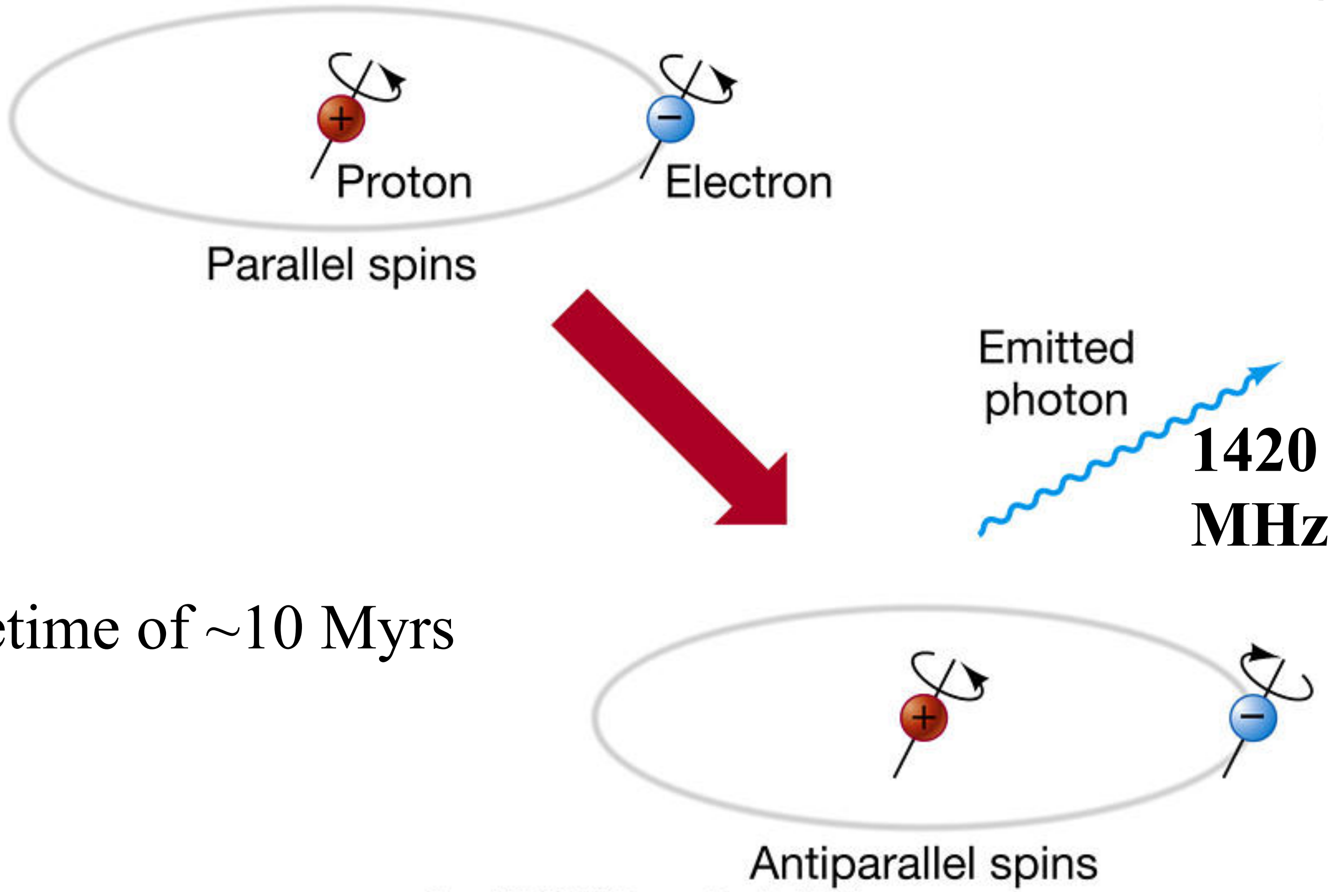

Lifetime of ~10 Myrs

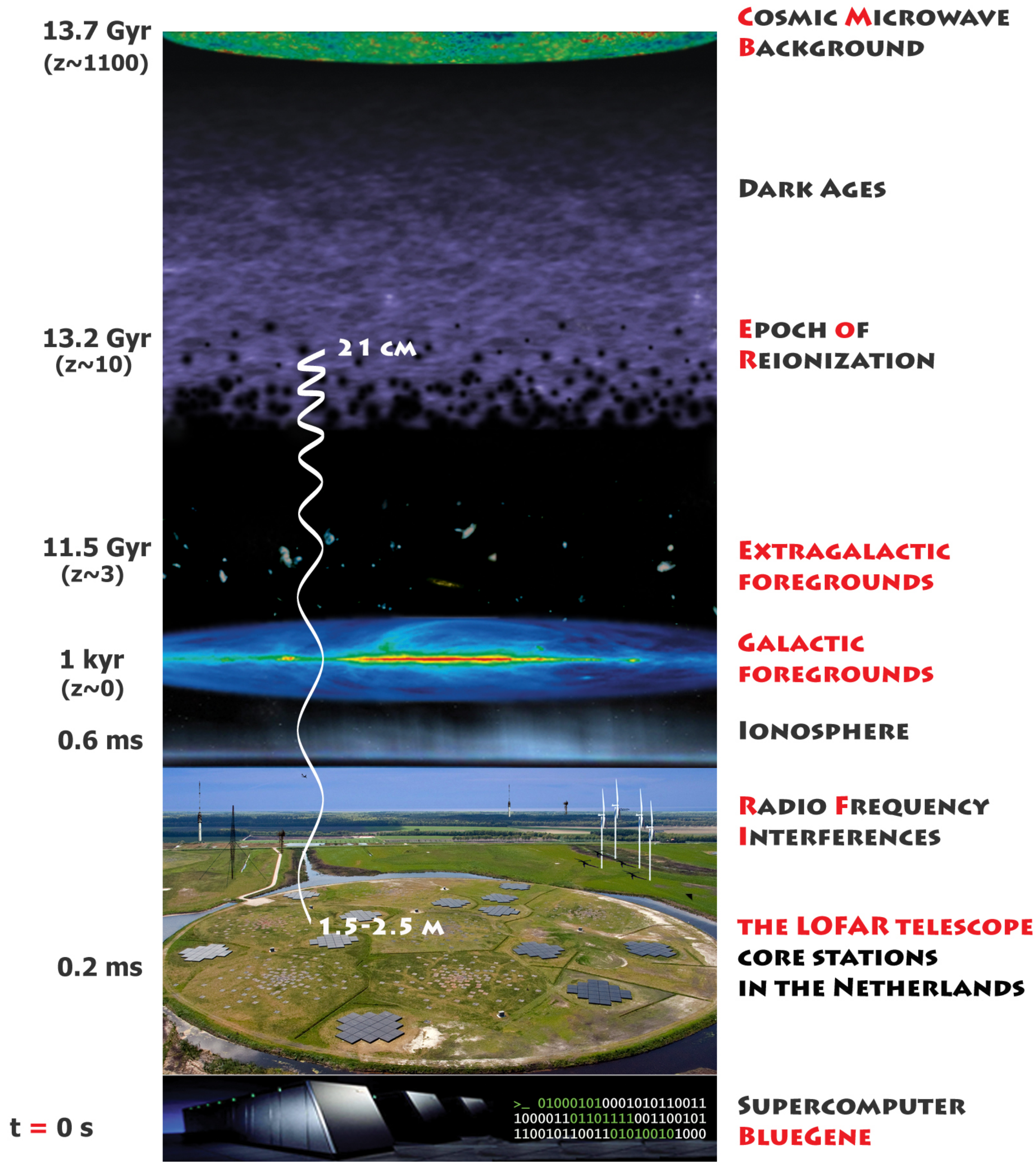

13.7 Gyr
(z~1100)
Cosmic Microwave Background
Dark Ages
13.2 Gyr
(z~10)
21 cm
Epoch of Reionization
11.5 Gyr
(z~3)
Extragalactic foregrounds
1 kyr
(z~0)
Galactic foregrounds
0.6 ms
Ionosphere
Radio Frequency Interferences
1.5-2.5 m
0.2 ms
the LOFAR telescope
core stations
in the Netherlands
t = 0 s
>_ 01000101000101011001
10000110110111100110010
11001011001101010010100
Supercomputer BlueGene

International LOFAR Telescope (ILT)

Core Station

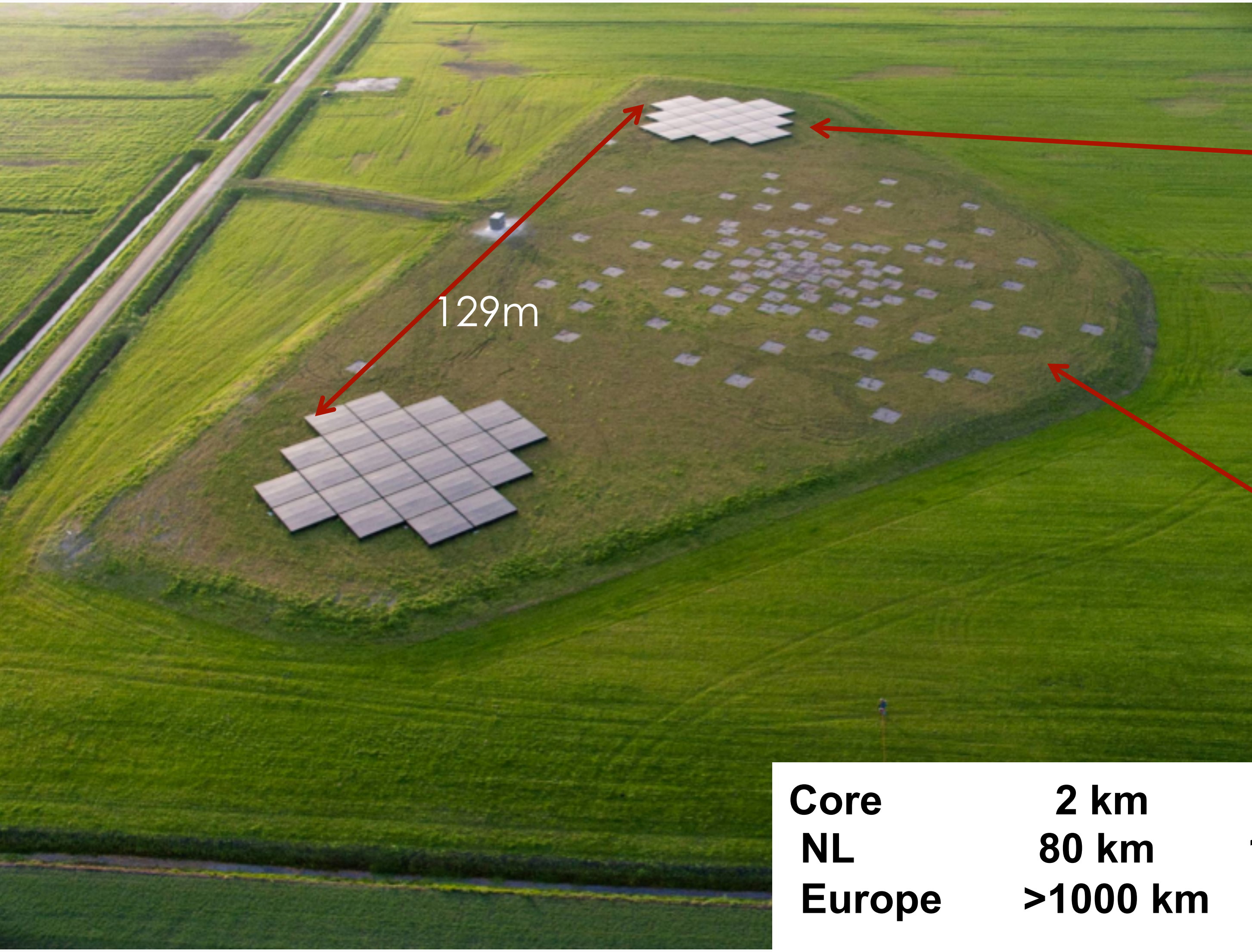

HBA:
High frequency Tiles
115 - 240 MHz

LBA:
Low frequency dipoles
30 - 90 MHz

Core	**2 km**	**24 (x2) stations**
NL	**80 km**	**18+ stations**
Europe	**>1000 km**	**12+ stations**

Total # of HBA dipoles: ~ 50000.

LOFAR from Space

The LOFAR EoR members

What can LOFAR Observe of the EoR?

Slices through a hydro-simulation

Iliev et al. 2012

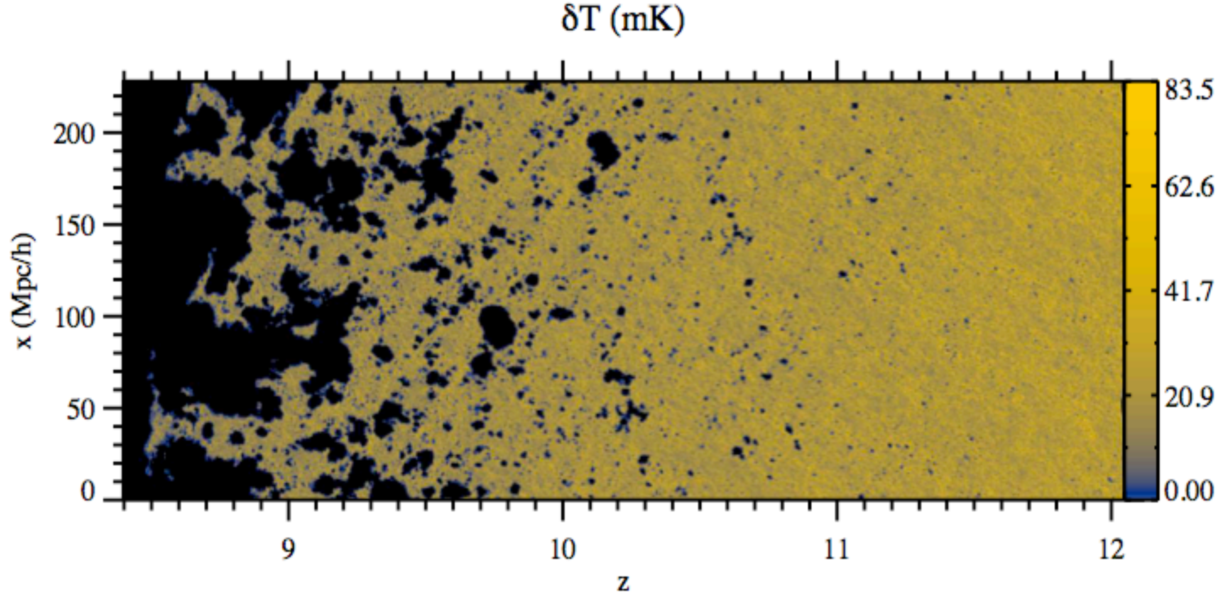

What LOFAR could see.

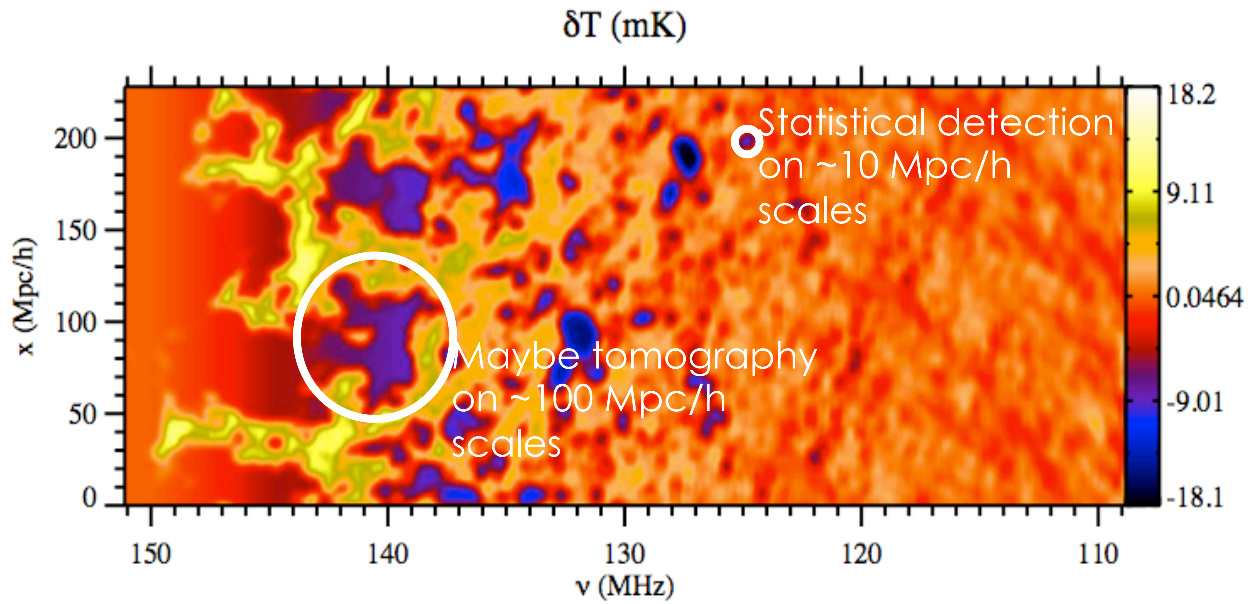

Measuring Redshifted HI: Challenges

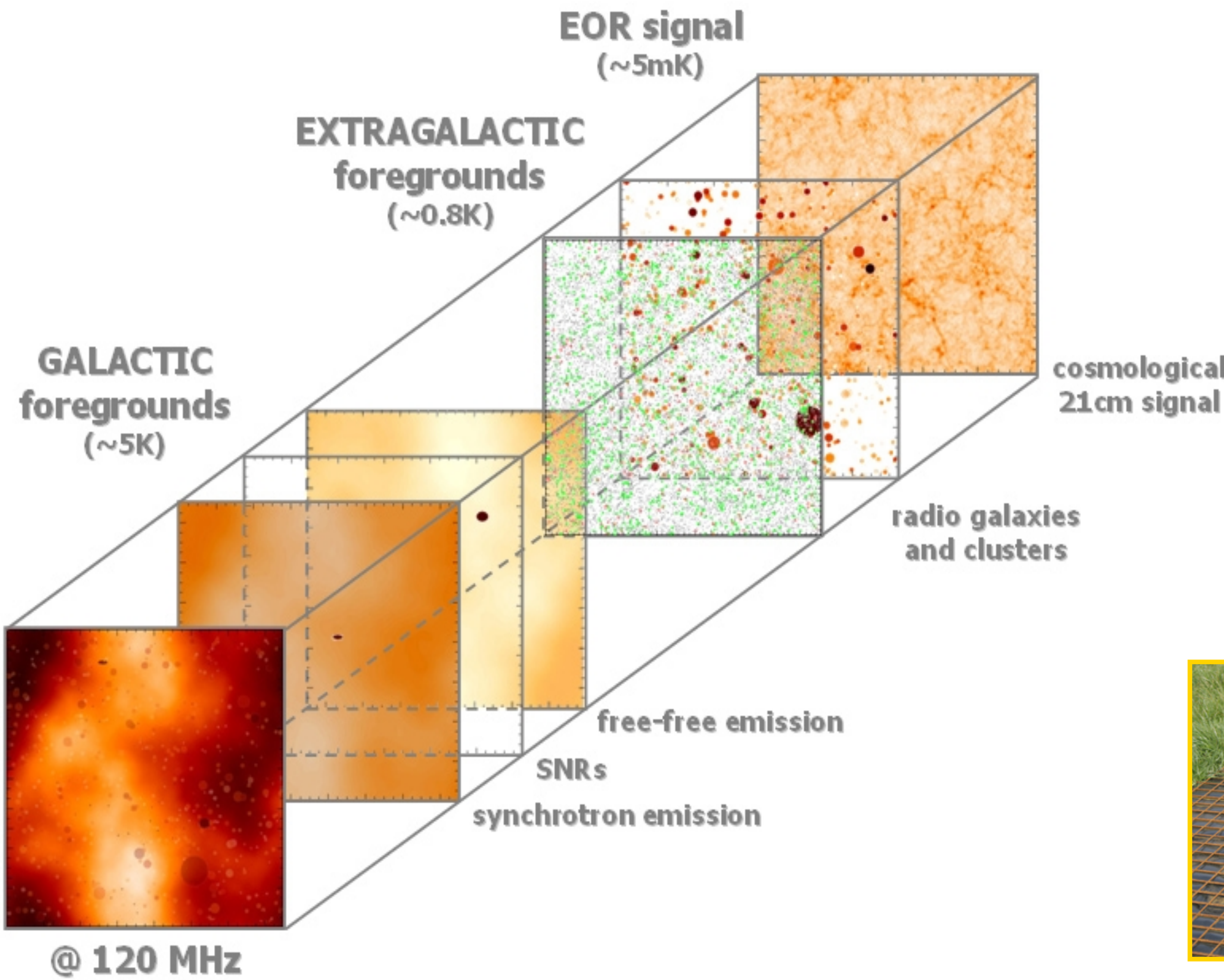

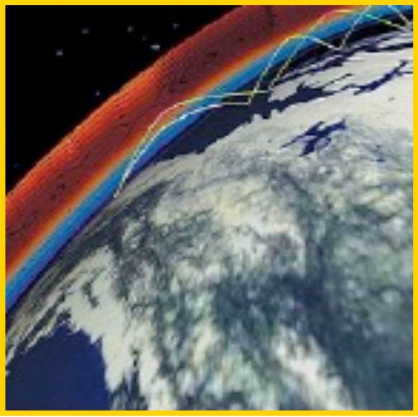

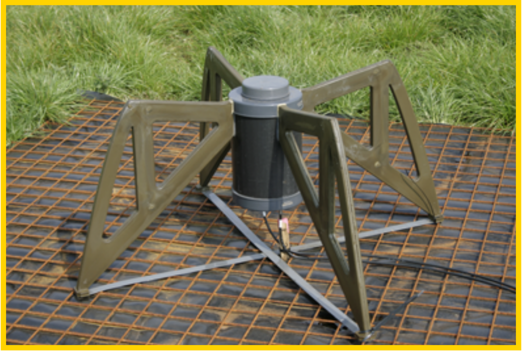

Statistical detection of the EoR signal: Variance Evolution

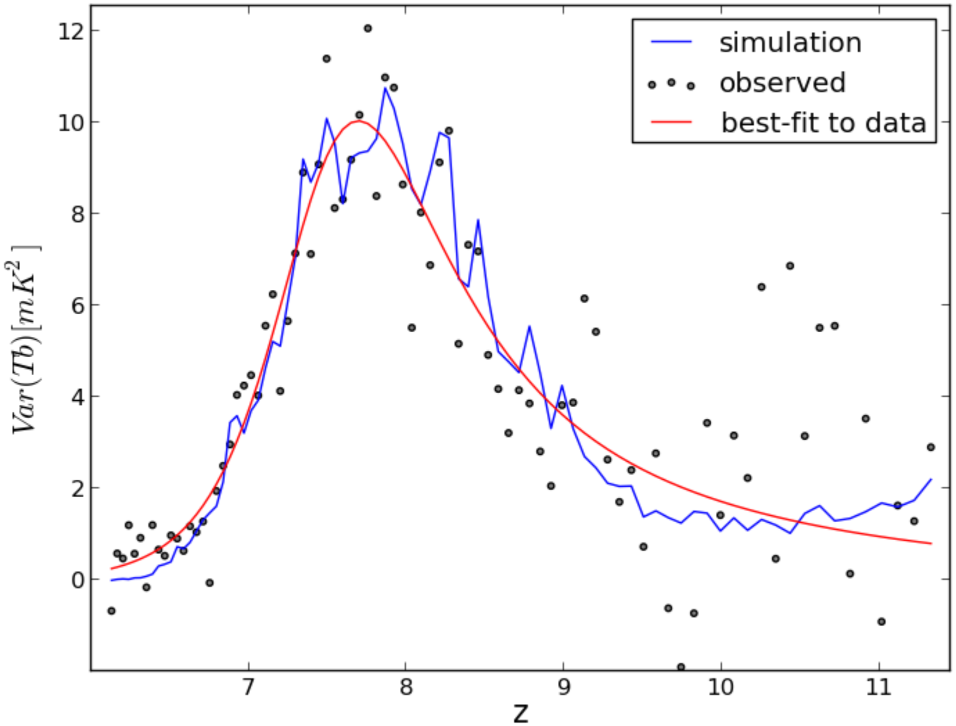

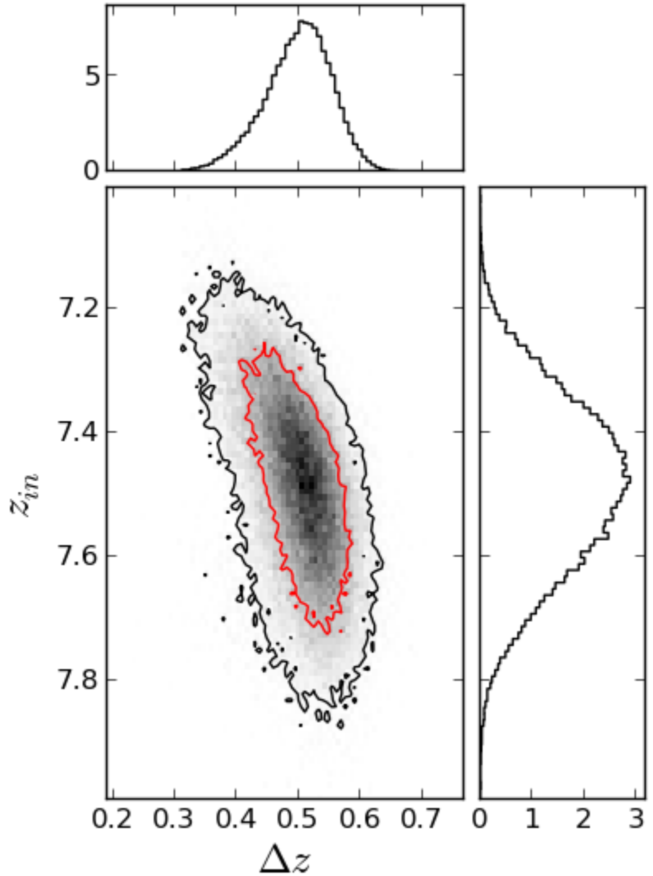

Patil et al. (in prep.), Jelic et al., 2008; Harker et al., 2010; Chapman et al. 2012,2013

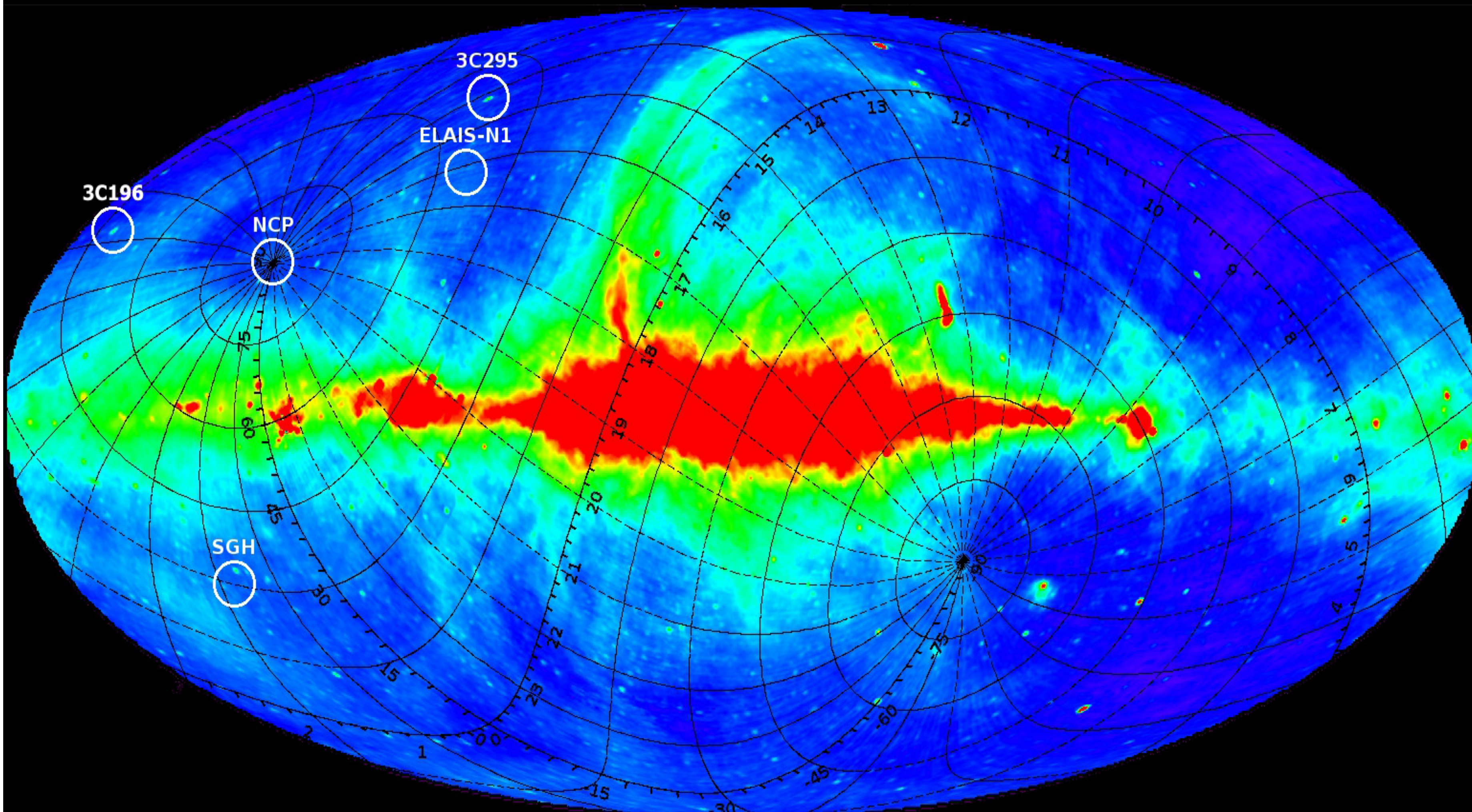

Haslam 408MHz map

3C196 field: Magentic fields in the Galaxy

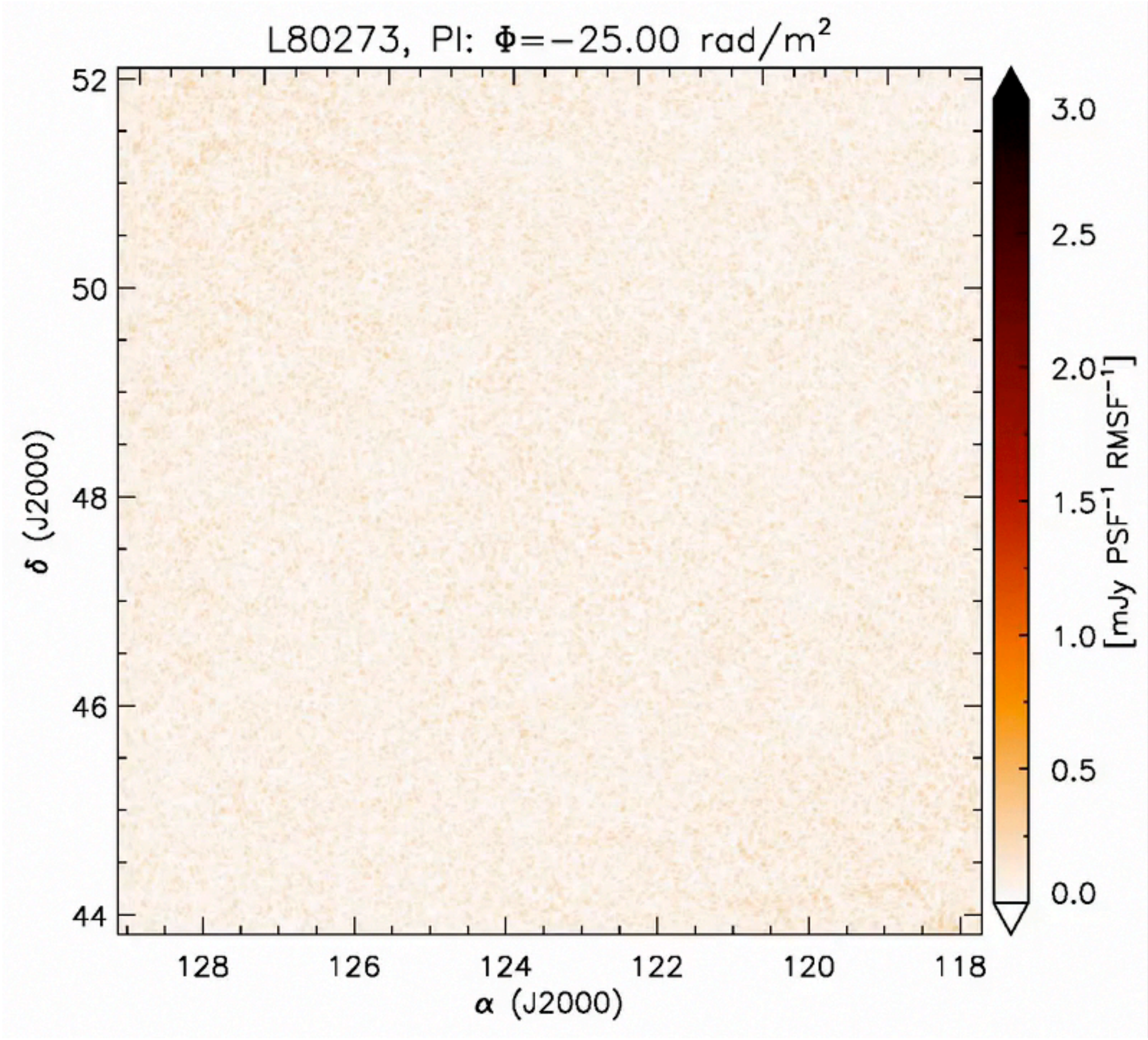

Jelic et al 2015

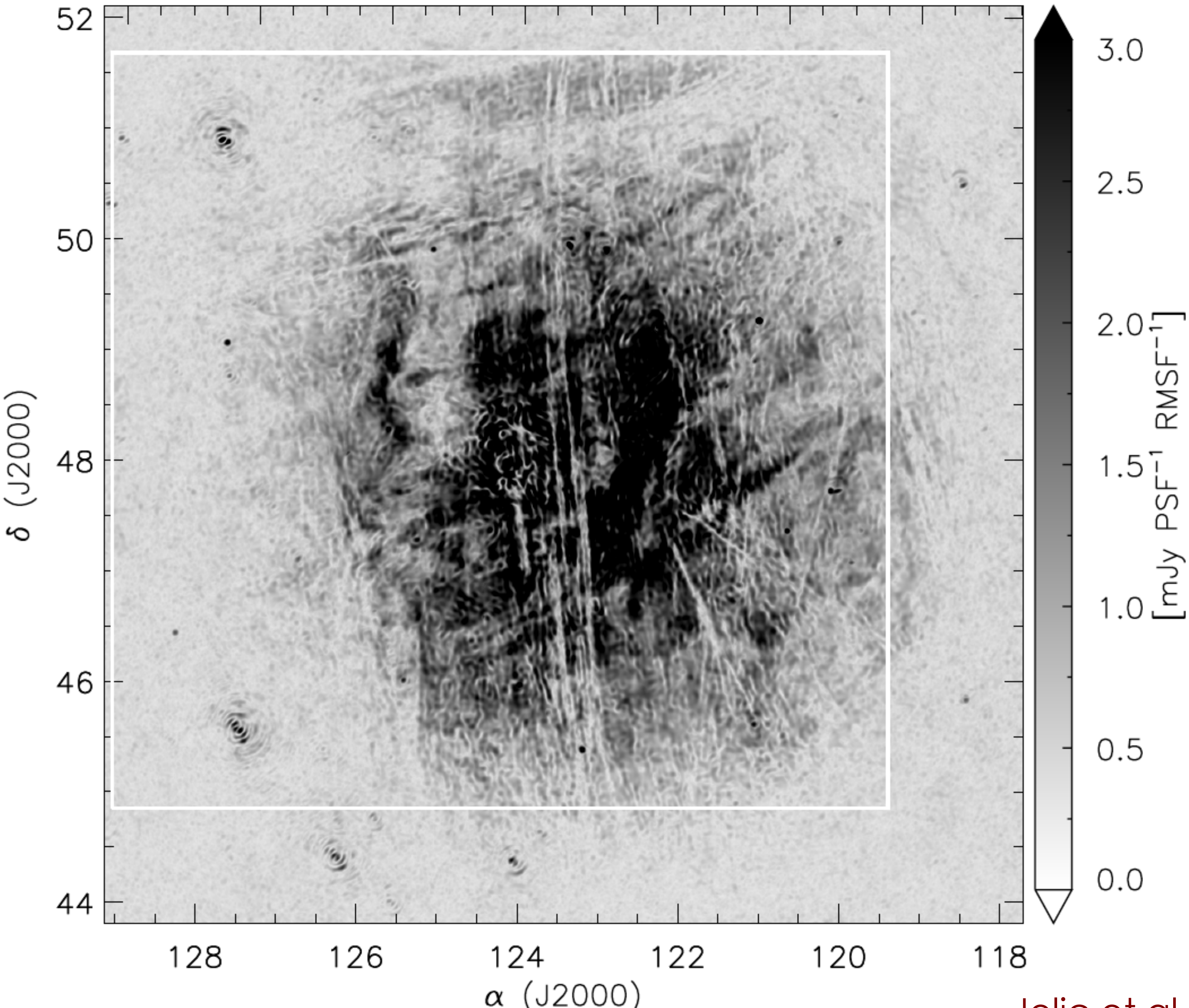

Jelic et al 2015

ISM magnetic/Faraday depth correlation (LOFAR vs. Planck)

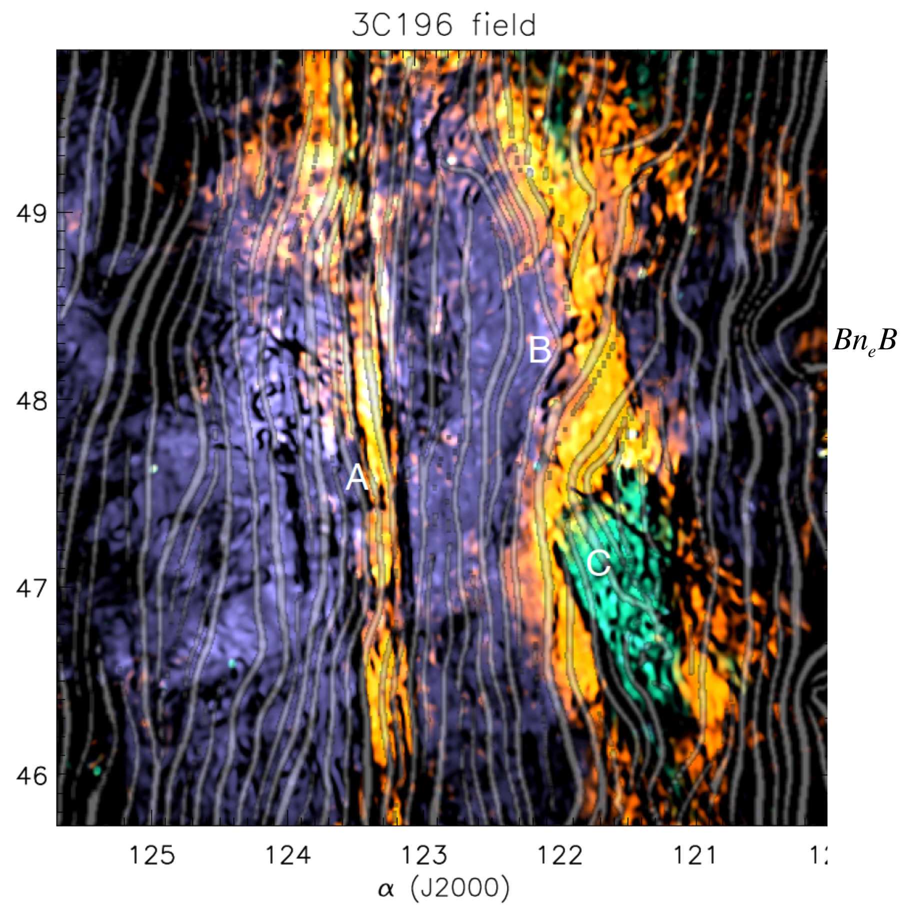

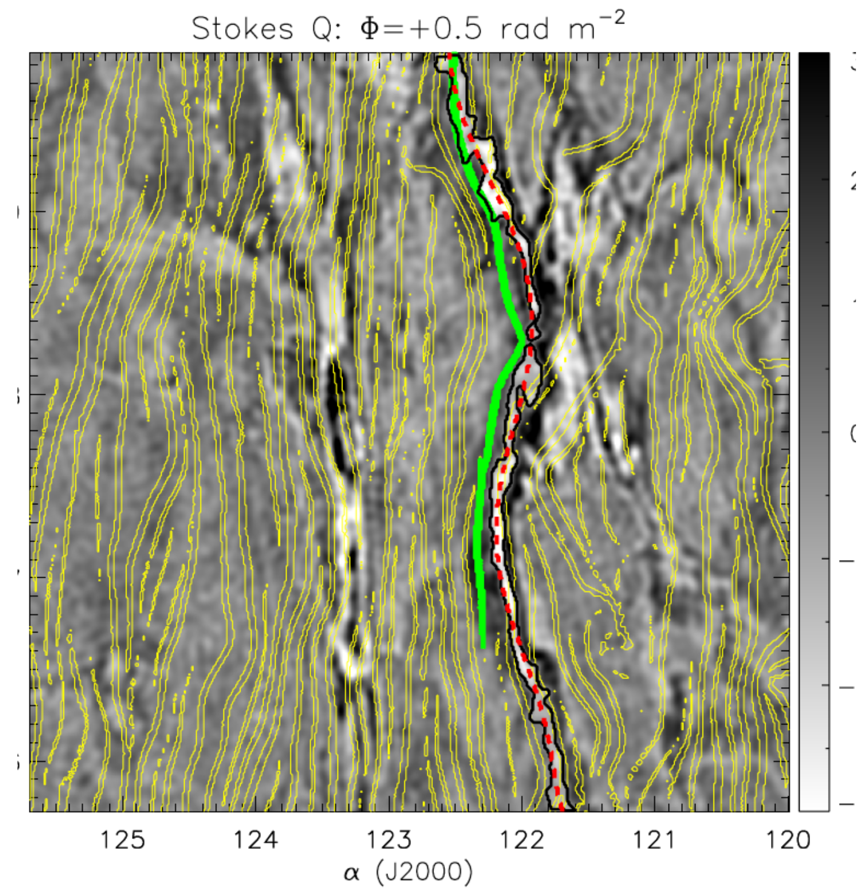

Zaroubi et al 2015

Image quality: NCP

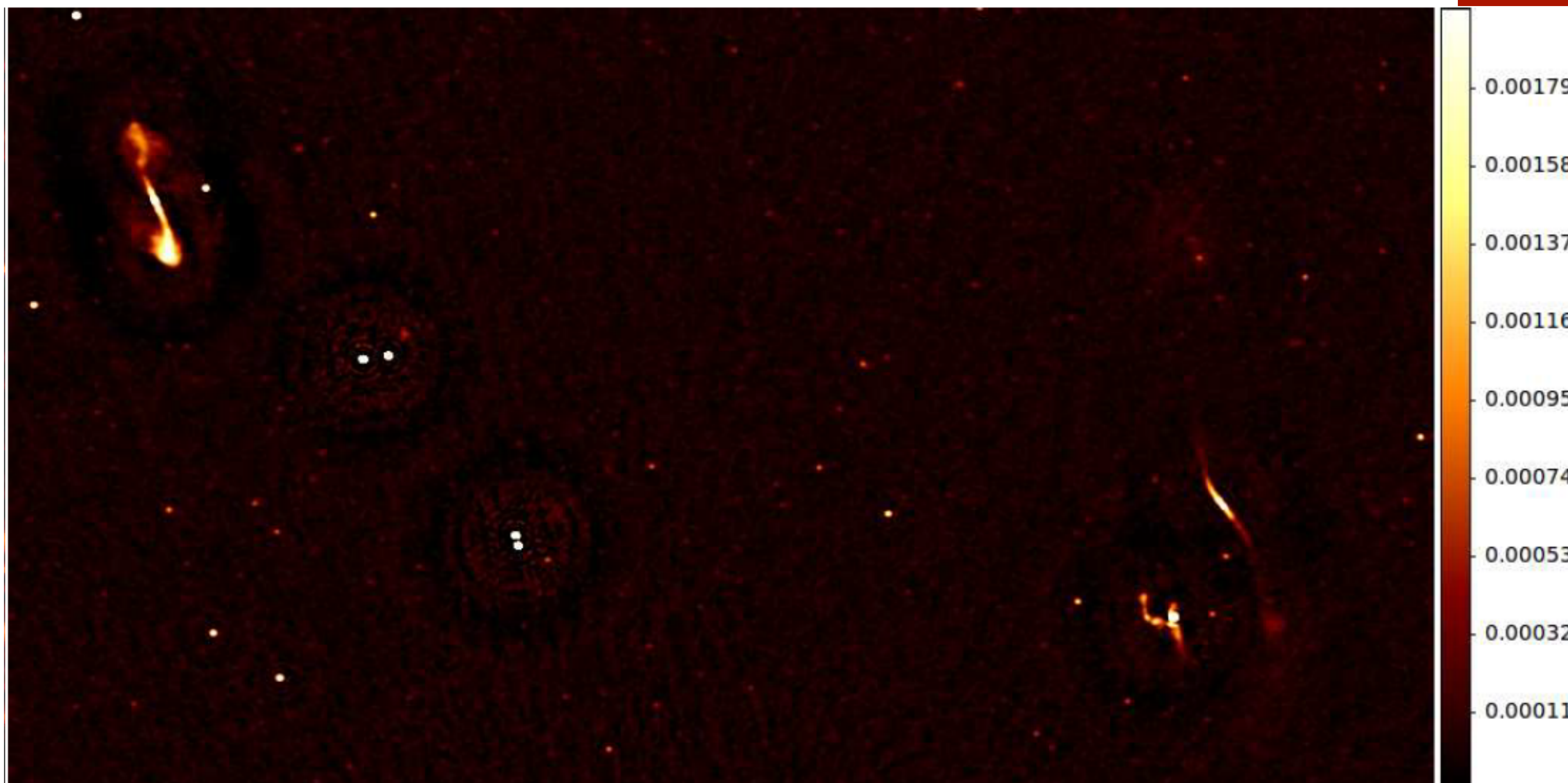

25-30 μJy, 6″ PSF, Dec 2012-Feb 2013, 80 km array, 0.5×0.25 degrees

UPPER LIMITS ON THE 21-CM EPOCH OF REIONIZATION POWER SPECTRUM FROM ONE NIGHT WITH LOFAR

A.H. Patil[1], S. Yatawatta[1,2], L.V.E. Koopmans[1,†], A.G. de Bruyn[2,1], M. A. Brentjens[2], S. Zaroubi[1,11], K. M. B. Asad[1], M. Hatef[1], V. Jelić[1,8,2], M. Mevius[1,2], A. R. Offringa[2], V.N. Pandey[1], H. Vedantham[9,1], F. B. Abdalla[7,13], W. N. Brouw[1], E. Chapman[7], B. Ciardi[4], B. K. Gehlot[1], A. Ghosh[1], G. Harker[3,7,1], I. T. Iliev[10], K. Kakiichi[4], S. Majumdar[12], M. B. Silva[1], G. Mellema[5], J. Schaye[6], D. Vrbanec[4], S. J. Wijnholds[2]

[1]Kapteyn Astronomical Institute, University of Groningen, P.O. Box 800, 9700 AV Groningen,The Netherlands

[2]ASTRON, P.O.Box 2, 7990 AA Dwingeloo, The Netherlands

[3]Center for Astrophysics and Space Astronomy, Dept. of Astrophysics and Planetary Sciences, University of Colorado at Boulder, CO 80309, USA

[4]Max-Planck Institute for Astrophysics, Karl-Schwarzschild-Straße 1, 85748 Garching, Germany

[5]Department of Astronomy and Oskar Klein Centre for Cosmoparticle Physics, AlbaNova, Stockholm University, SE-106 91 Stockholm, Sweden

[6]Leiden Observatory, Leiden University, PO Box 9513, 2300RA Leiden, The Netherlands

[7]Department of Physics and Astronomy, University College London, Gower Street, WC1E 6BT, London, UK

[8]Ruđer Bošković Institute, Bijenička cesta 54, 10000 Zagreb, Croatia

[9]Cahill Center for Astronomy and Astrophysics, MC 249-17, California Institute of Technology, Pasadena, CA 91125, USA

[10]Astronomy Centre, Department of Physics & Astronomy, Pevensey II Building, University of Sussex, Brighton BN1 9QH, UK

[11]Department of Natural Sciences, The Open University of Israel, 1 University Road, PO Box 808, Ra'anana 4353701, Israel

[12]Department of Physics, Blackett Laboratory, Imperial College, London SW7 2AZ, UK

[13]Department of Physics and Electronics, Rhodes University, PO Box 94, Grahamstown, 6140, South Africa

IN PRESS !!

NCP field

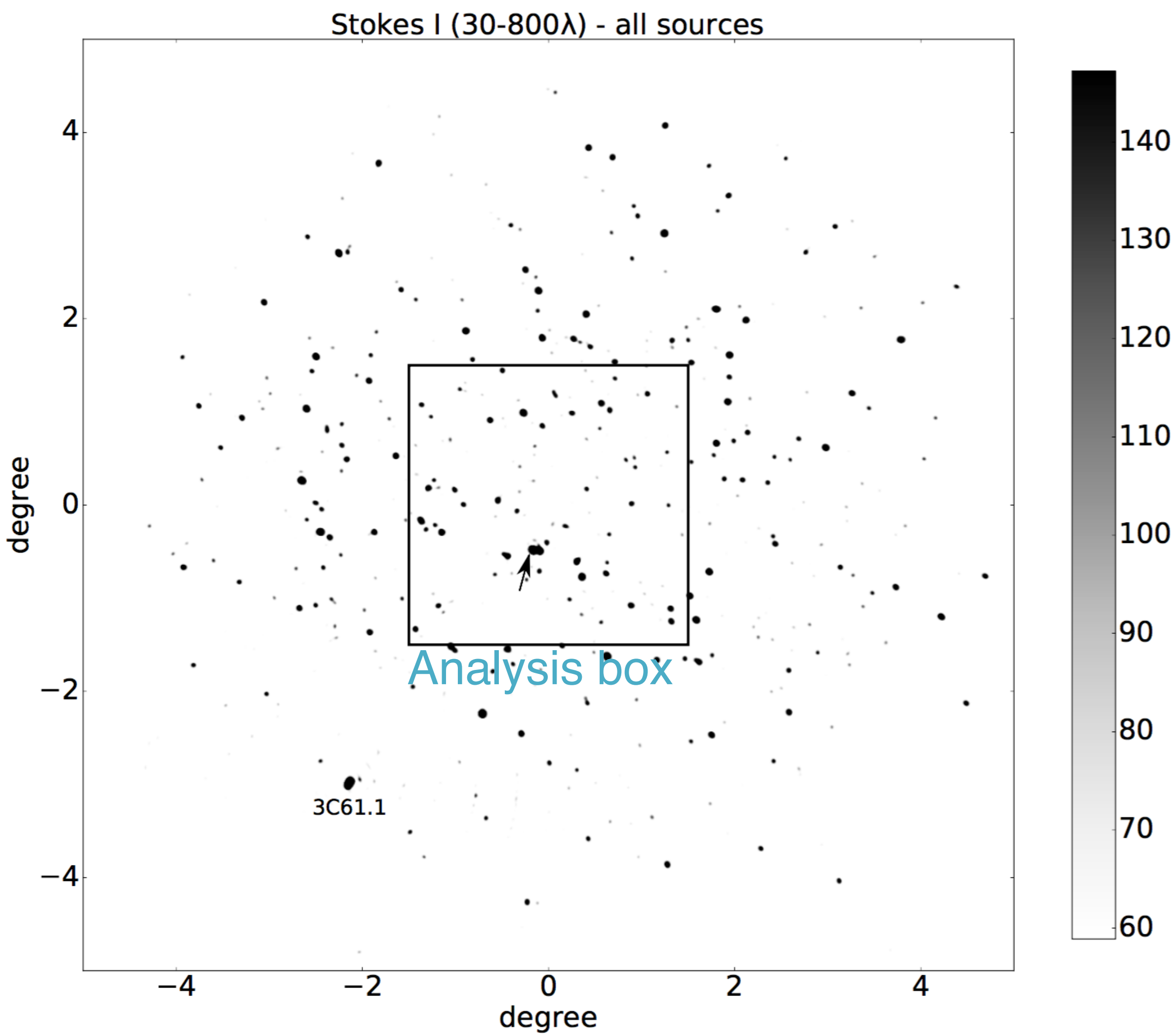

Figure 1. A relatively narrow-band continuum (134.5-137.5 MHz) LOFAR-HBA image of 10° × 10° of the North Celestial Pole (NCP) field, centered at dec +90.0°. Baselines between 30-800λ were included, using uniform weighting. No sources have been subtracted and the image is cleaned to a level sufficient to show the brightest few hundred sources above 60 mJy. The 3° × 3° box delineates the area where we measure the power spectra. The bright extended source in the lower-left is 3C61.1 (J0222+8619), discussed in the text. The bright (7.2 Jy) compact source near the NCP is indicated by an arrow. The intensity units are mJy/PSF (see text). Right Ascension increases clockwise; RA=00h is towards the bottom.

L90490

13-hr integration over ~74 MHz with all LOFAR HBA stations (Feb 11/12, 2013)

Phase Centre ($\alpha, \delta; J2000$)	0^h, +90°	
Minimum frequency	115.039	MHz
Maximum frequency	189.062	MHz
Target bandwidth	74.249	MHz
Stations (core/remote)	48 / 13	
Raw data volume L90490	61	Tbyte
Sub-band (SB) width	195.3125	kHz
Correlator channels per SB	64	
Correlator integration time	2	s
Channels per SB after averaging	15, 3, 3, 1	
Integration time after averaging	2, 2, 10, 10	s
Data size (488 sub-bands)	50	Tbyte

Table 1. Observational and correlator set up of LOFAR-HBA observations of the North Celestial Pole (NCP).

Rough processing outline

- Analysis starts with standard NDPPP calibration/flagging of known (tabulated) issues
- AOFlagger (~5% loss of data)
- Sky-model is built of ~21,000 components over 122 "clusters" (directions) out to about 19° from NCP/
- Calibration on baselines >250λ, analysis on baselines 50-250λ; avoid removal of diffuse emission
- Data is "direction-independently" calibrated using
- Direction dependent calibration with SageCal-COFinal step before PS analysis on 3 redshift windows is diffuse FG removal with GMCA (see later).

Parameter	Value	Comments
Sky-model components	~20,800	Compact
Flux-limit sky model	~3 mJy	
Order P_n^S source spectra	3	Polynomial
DI-Calibration directions	2	
DD-Calibration directions	122	Source clusters
Calibration baselines	≥250 λ	
Order B_n^G gain regul.	3	Bernstein Polynomial
Solution interval	10 min	
uv-grid cells	$4.58 \times 4.58\ \lambda$	
w-slices	128	
EoR Imaging baselines	50-250 λ	
EoR Imaging FoV	$3^\circ \times 3^\circ$	
EoR pixel size	$0.5' \times 0.5'$	
EoR Imaging Resolution	~10'	FWHM
EoR Freq. Resolution	~60 kHz	
Redshift range #1	7.9 – 8.7	
Freq. range	146.8 – 159.3 MHz	
GMCA components	6/0	Stokes I/V.
Redshift range #2	8.7 – 9.6	
Freq. range	134.3 – 146.8 MHz	
GMCA components	6/2	Stokes I/V.
Redshift range #3	9.6 – 10.6	
Freq. range	121.8 – 134.3 MHz	
GMCA components	8/2	Stokes I/V.

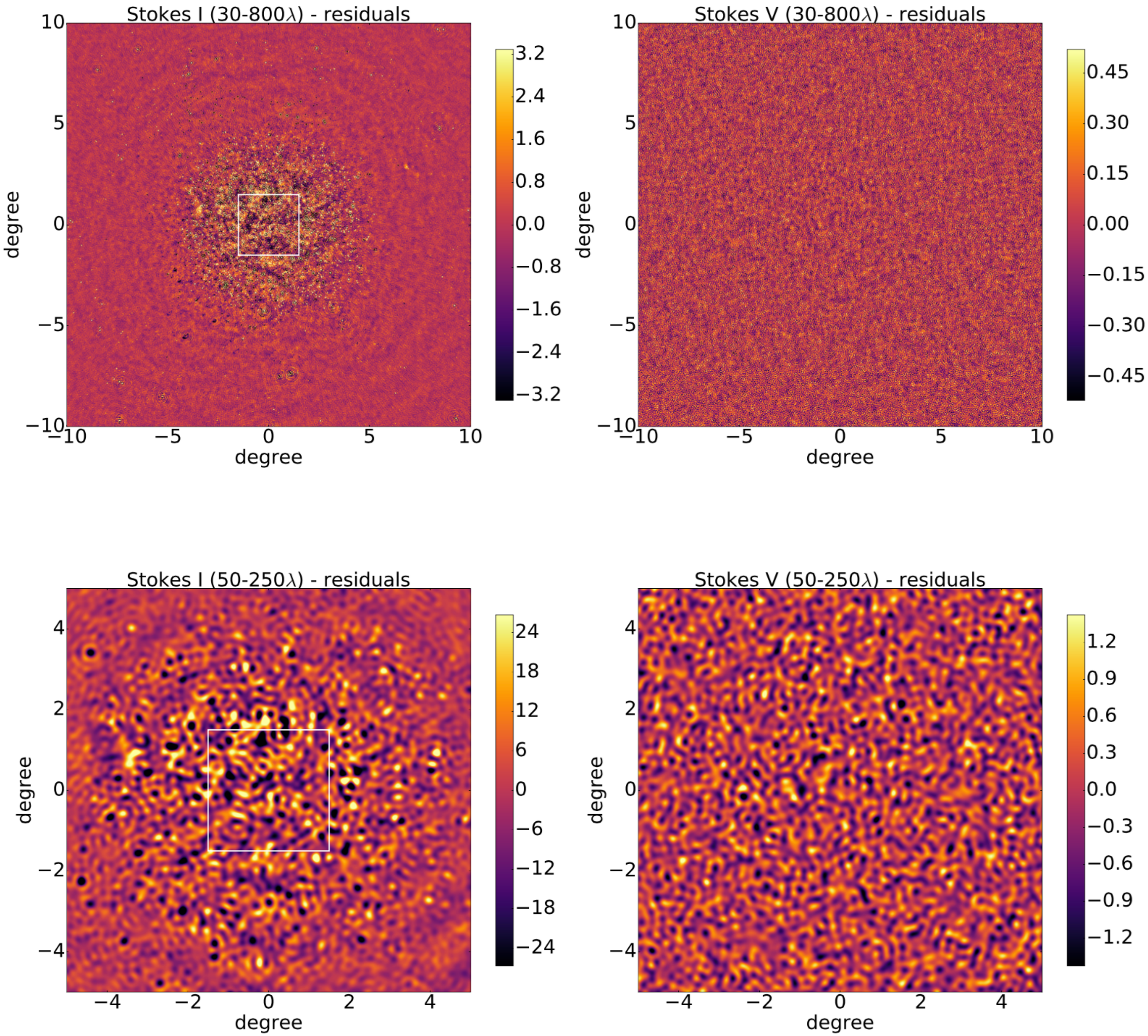

Stokes I (left)
Stokes V (right)
@ 2 resolutions
(~12, 4 arcmin)

After SageCal-CO and removal sky-model.
Stokes I is confusion limited/Stokes V is thermal-noise limited.

Diffuse emission is hard to see

Figure 2. Stokes I and Stokes V images after sky-model subtraction for the baseline ranges 30-800λ (top panels) and 50–250λ (bottom panels). Sub-bands with frequencies between 121 and 134 MHz went into these images. Note the reduction in the displayed field-of-view from 20×20° to 10×10°. Intensity units are in mJy/PSF and the scale range is set by plus and minus three times the standard deviation over the full field in all images. Note the noise-like structure in the two Stokes V images. i.e. a lack of any features. The Stokes I images, on the other hand, clearly show the LOFAR-HBA primary beam attenuation effects on the remaining diffuse emission. The level of this emission is limited by the classical confusion noise within the primary beam. The 3° × 3° box delineates the area where we measure the power spectra.

A spatial-frequency slice:

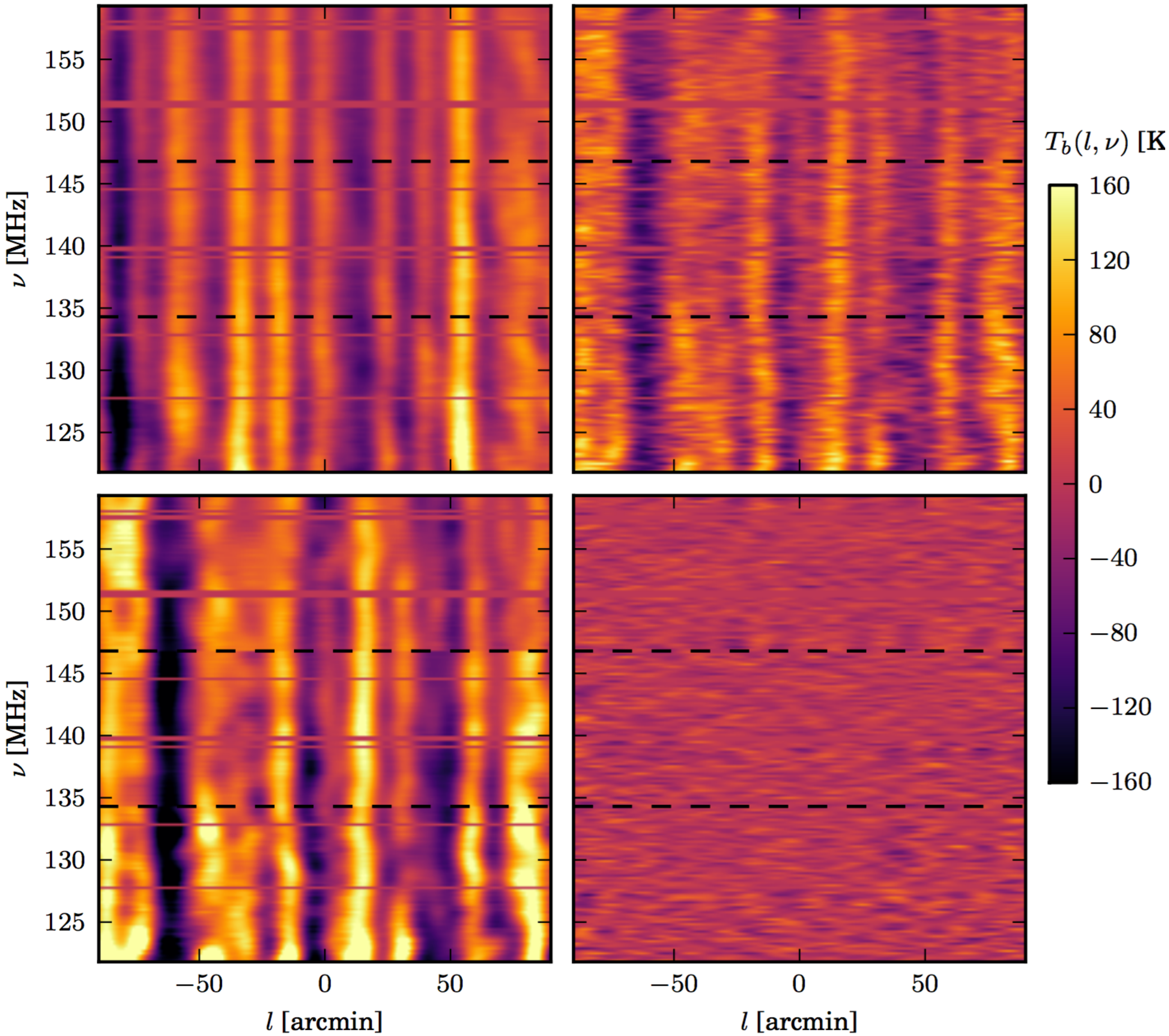

Figure 3. A slice across the centre of the 50–250λ Stokes-I data cube along the frequency direction. Top left: slice after *DI*-calibration with only 3C61.1 subtracted; the intensity scale, converted to brightness temperature, refers to this panel. Top right: after *DD*-calibration where the calibration sky model, consisting of compact sources, is subtracted with their respective direction-dependent gain solutions. The intensity scale is now multiplied by 10 for improved visualization; Bottom left: GMCA model (scale also multiplied by 10); Bottom right: GMCA residuals (scale multiplied by another factor of 20). The red horizontal bands are due to data lost due to RFI-flagging. The black dashed lines border the three redshift ranges. Note the factor ~200 reduction in intensity after GMCA.

(1) strong spectrally smooth sources before sky-model subtraction (upper left)
(2) Confusion noise of fainter source and diffuse emission (upper right)
(3) GMCA model of remaining FGs (lower left)
(4) Residuals after GMCA model subtraction (lower right)

Residuals look like noise, but they are not (there is excess variance beyond Stokes V).

The importance of sky-model subtraction after DD-calibration is illustrated in the power-spectra:

Lots of "leakage" in to the EoR window
no clean "EoR window" for LOFAR

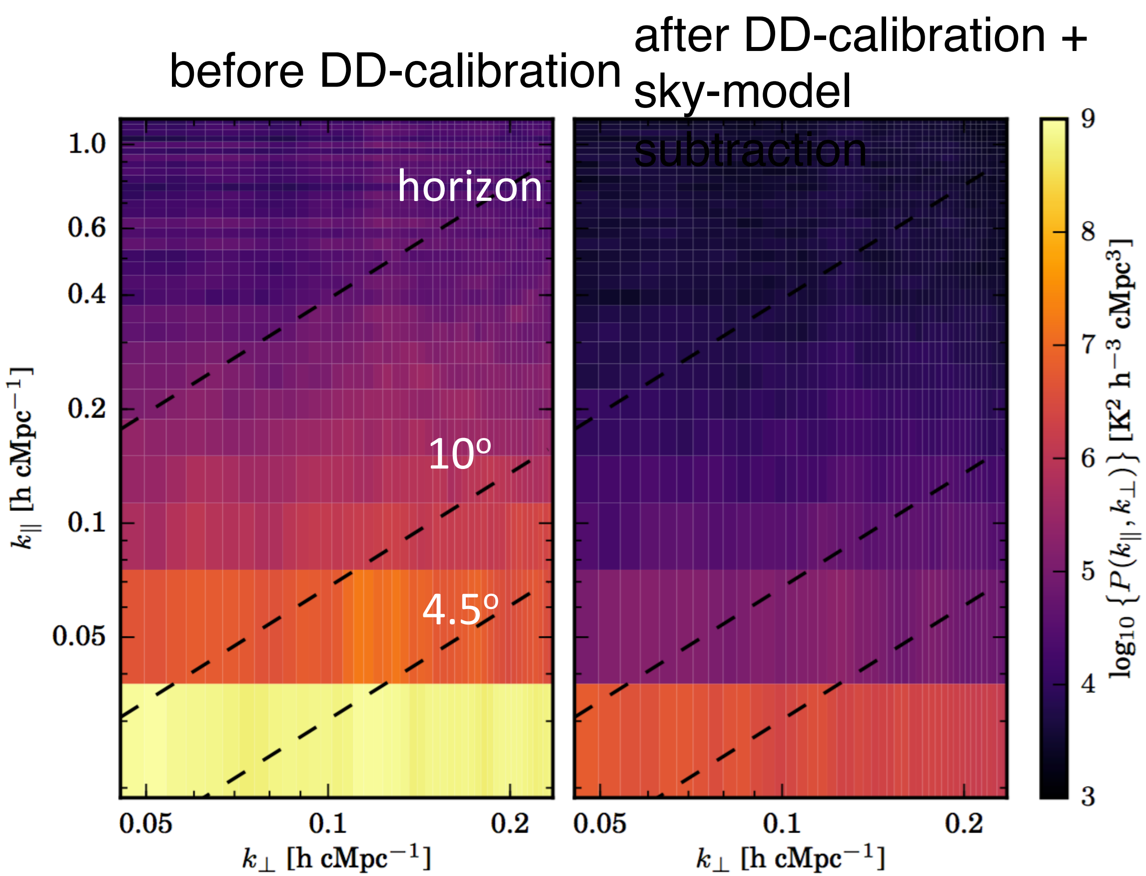

Figure 5. The Stokes-I power spectra for the redshift range $z = 9.6 - 10.6$, before (top left) and after (top right) *DD*-calibration with SageCal-CO, respectively. Note the large drop in power of the foregrounds at low $k_{\parallel}$ and the removal of substantial power above the wedge as well. The dashed slanted lines indicate, from bottom to top, the location of angular distances of 4.5° and 10° from the phase centre, and the maximum delay corresponding to the horizon as seen from the zenith. The ratio between these power spectra is shown in Fig. 5

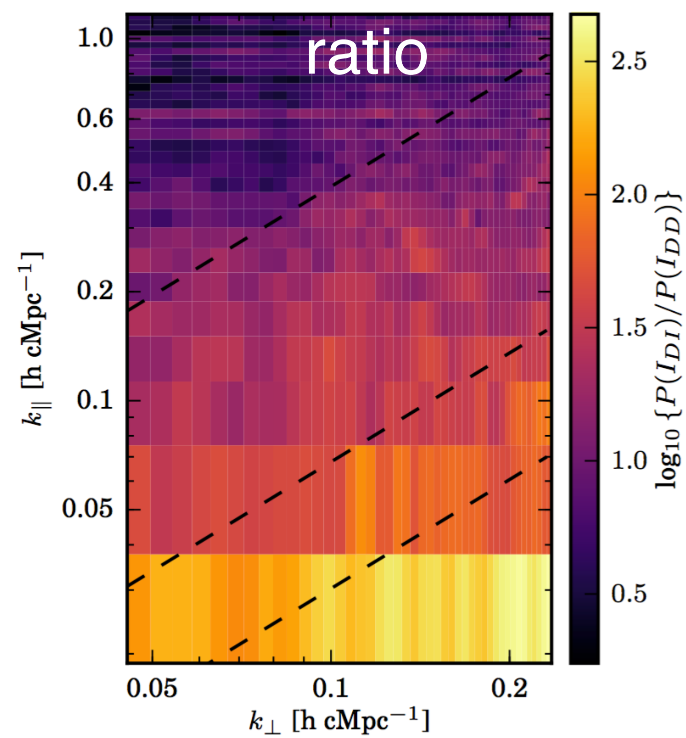

Figure 6. The ratio between the Stokes-I power before and after *DD*-calibration There is a drop of two orders of magnitude in power in the foregrounds at low $k_{\parallel}$. The dashed slanted lines indicate, from bottom to top, the location of angular distances of 4.5° and 10° from the phase center, and the maximum delay corresponding to the horizon as seen from the zenith.

Cylindrical Power-Spectra

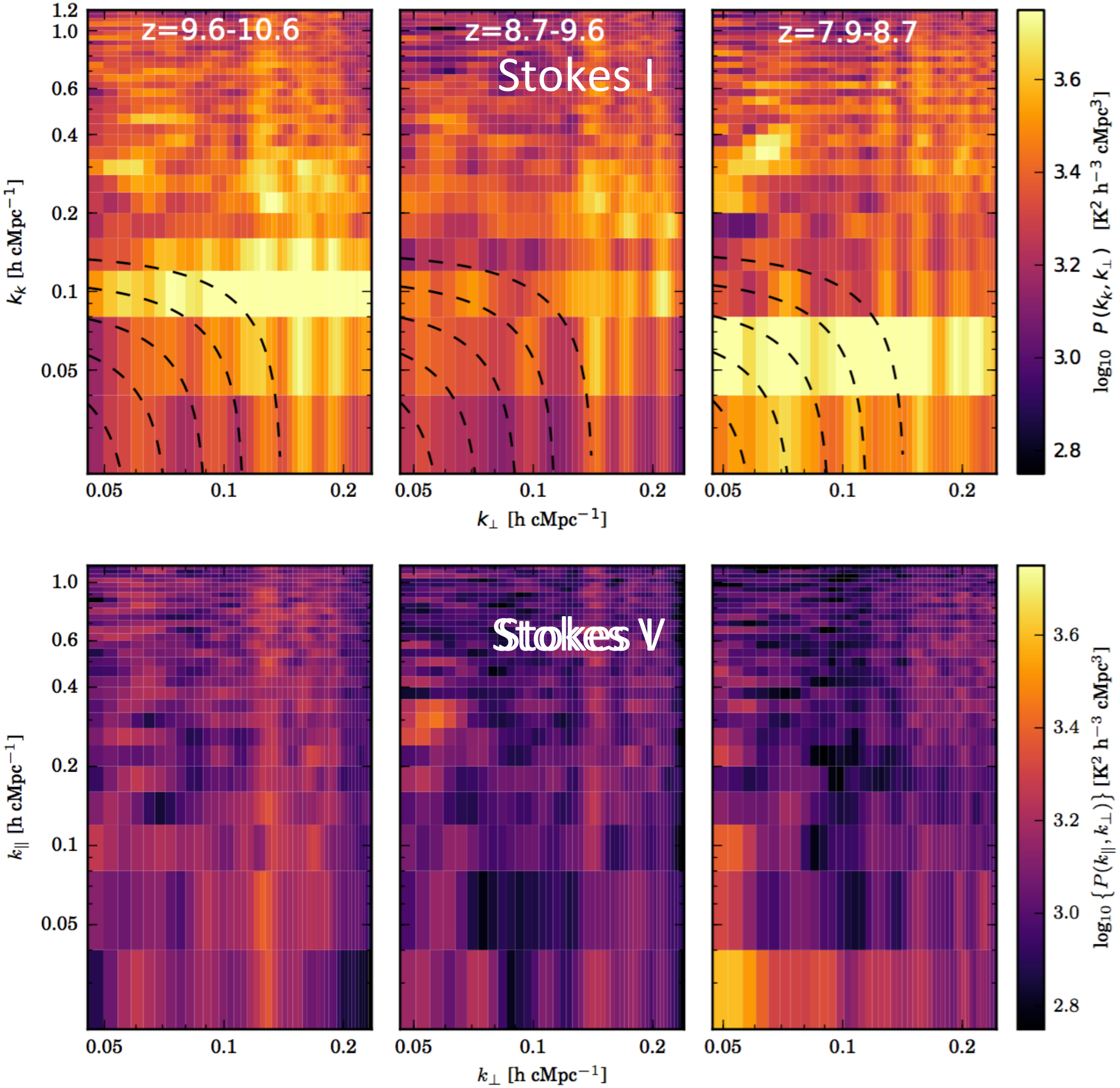

Figure 4. Stokes I (top) and V (bottom) cylindrical power spectra after sky model and GMCA-model subtraction, for L90490. From left to right are shown the redshift ranges $z = 9.6 - 10.6$, $z = 8.7 - 9.6$ and $z = 7.9 - 8.7$, respectively. The dashed curved lines in the Stokes I spectra refer to k values of 0.054, 0.067, 0.083, 0.103 and 0.128 for $z = 8.7 - 9.6$ and only slightly different values for the other redshift bins. It is along these lines that we form the spherically averaged power spectra.

(1) Removal of FG
(2) residuals are left around $k_{||}$ ~0.05-0.1
(3) Stokes I show "excess variance" on all scale by about factor ~2.
(4) Stokes V is relatively clean and close to thermal (but not fully, about

Residuals look like noise, but they are not (there is excess variance beyond Stokes V).

Causes could be:

(1) Leverage
(2) Gain errors on long baselines due to:
    a. Ionospheric errors
    b. Residual sources and their side-lobes

Ratio of Stokes I over Stokes V appears rather flat over the cylindrical power spectrum (apart from few bands).

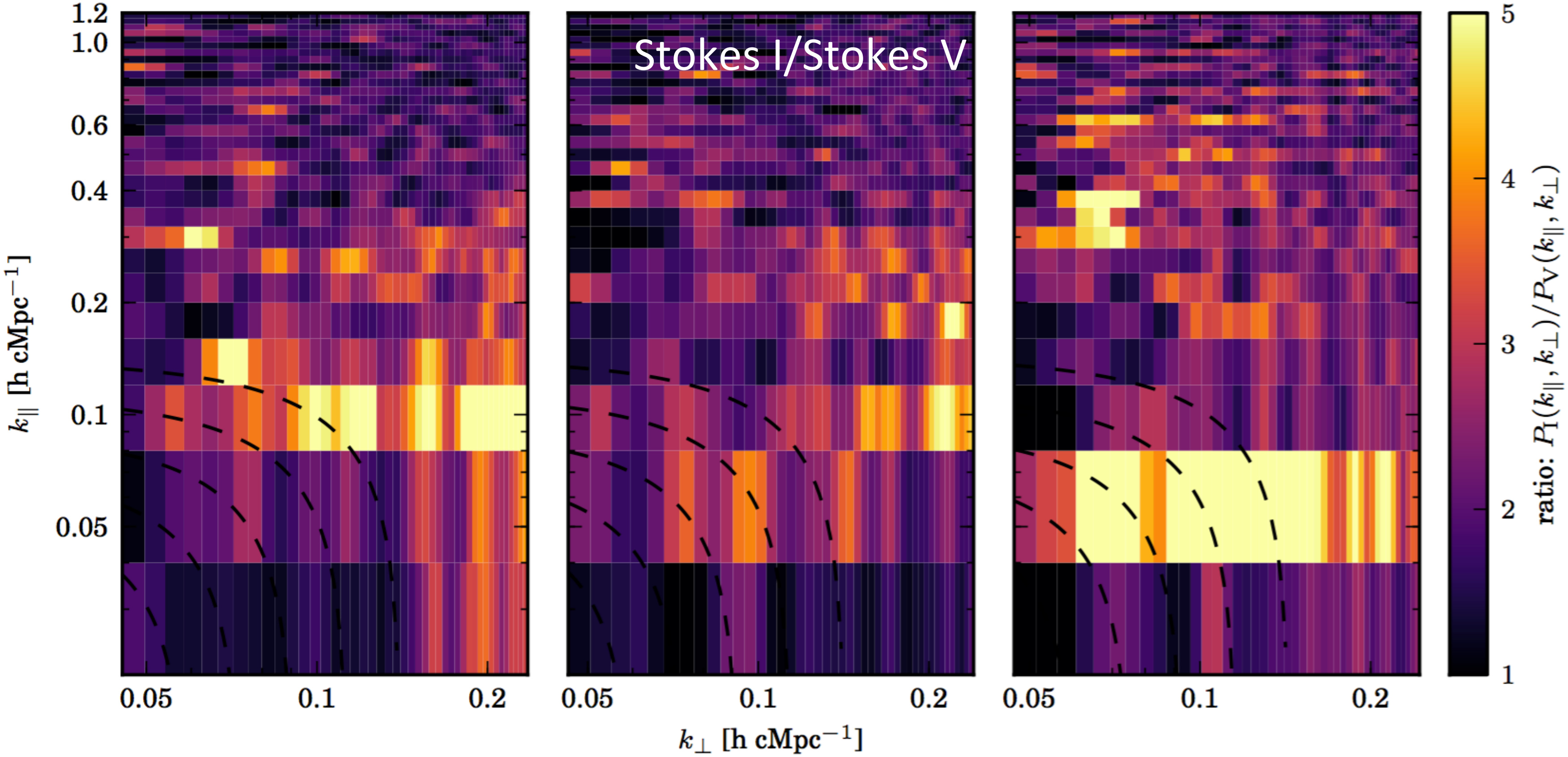

Figure 7. The Stokes I over V power spectra ratios for the redshift ranges $z = 9.6 - 10.6$, $z = 8.7 - 9.6$ and $z = 7.9 - 8.7$, respectively.

Spherical Power Spectra

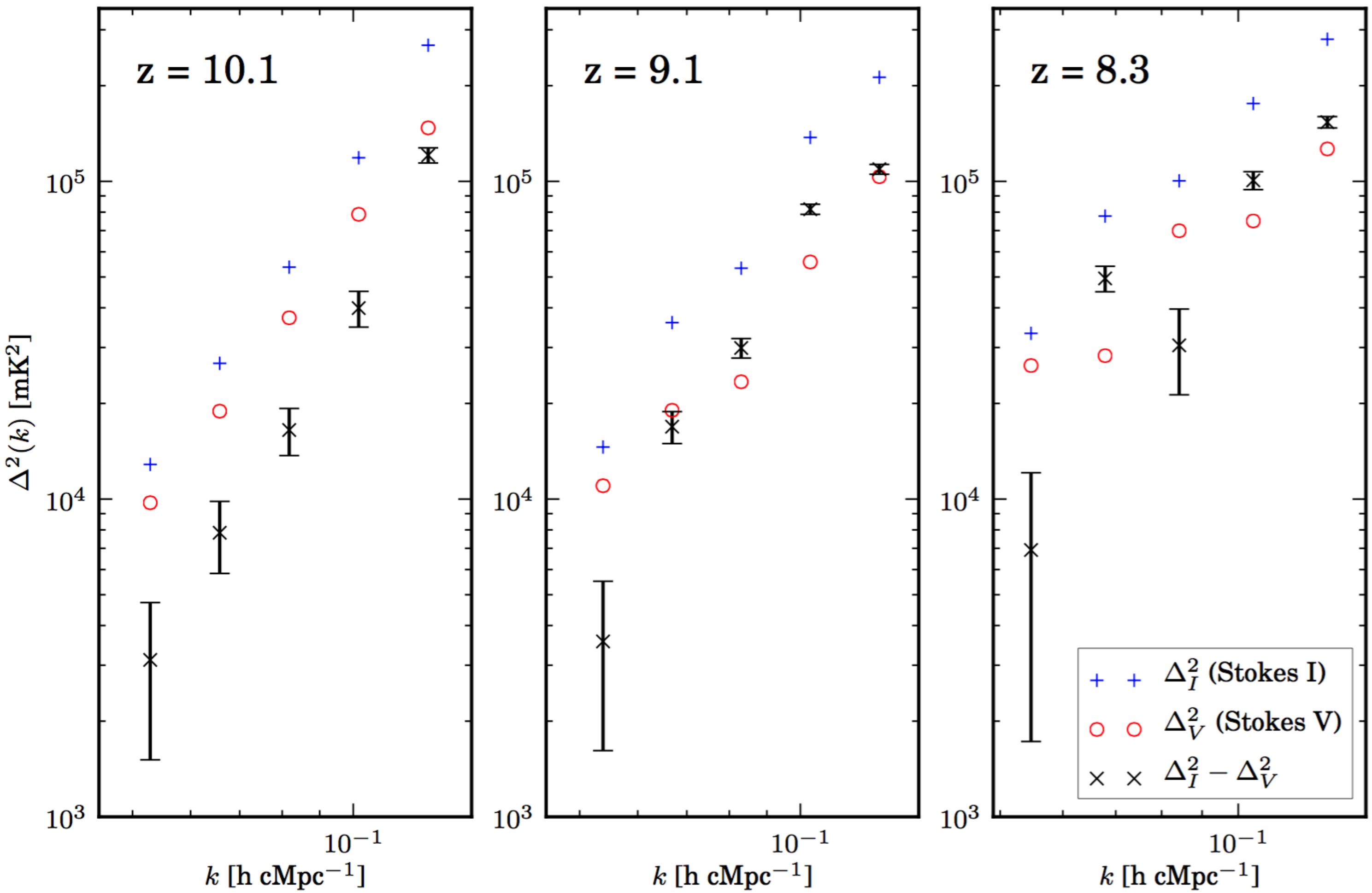

Figure 8. The spherically averaged Stokes I and V power spectra after GMCA for L90490; From left to right are shown the redshift ranges $z = 9.6 - 10.6$, $z = 8.7 - 9.6$ and $z = 7.9 - 8.7$ from left to right, respectively. The mean redshifts are indicated in the panels.

Spherical Power Spectra

- Although we have excess variance, we only give 2-sigma upper limits (incl. excess)
- Without excess variance we would have reached ~(57mK)^2 at z~10 and k~0.05
- We go less deep at higher-frequencies (issues with FG removal ?).

k h cMpc^{-1}	$z = 7.9 - 8.7$ mK^2	$z = 8.7 - 9.6$ mK^2	$z = 9.6 - 10.6$ mK^2
0.053	$(131.5)^2$	$(86.4)^2$	$(79.6)^2$
0.067	$(242.1)^2$	$(144.2)^2$	$(108.8)^2$
0.083	$(220.9)^2$	$(184.7)^2$	$(148.6)^2$
0.103	$(337.4)^2$	$(296.1)^2$	$(224.0)^2$
0.128	$(407.7)^2$	$(342.0)^2$	$(366.1)^2$

Table 3. Δ^2_{21} upper limits at the 2-σ level.

Cause of Excess Variance ?

Work by Patil et al (2016), and Barry et al. (2016), as well as correlation with ionospheric effect seem to point at a complex issue:

(1) Incomplete and DD gains onn long baselines when applied to calibrate baselines at 50-250λ and can cause excess variance.
(2) It correlates over ~MHz in the frequency direction expected from side-lobe noise from sources about 10^{o} away from phase center
(3) Excess variance seems to be less if data with stronger ionospheric effects are excized.
(4) Ionosphere on baselines>r_{diff}

It seems that excess noise is the combined effect of an incomplete sky model with ionospheric effects on longer baselines, causing (phase randomized) gain errors to be transferred to shorter baselines. This seems to explain many of the things we see (in qualitative terms) and they are effects that we know exists.

Improvements

(1) Reduce excess variance by using more “smooth” gain solutions on the longer baselines and possible reduce the range of long baselines.

(2) Include I, Q & U diffuse emission models such that short baselines can be used in the calibration. Is known to lead to less excess variance.

(3) Improve FG removal further: GMCA/GRP

(4) Include the 129m baselines that share electronics cabinet (currently not used). This can improve sensitivity on k~0.03-0.05 by factors >>2.

(5) Further improve compact sky-model

(6) Separate amplitude and phase solution time scales.

Current extrapolations (~100 nights) would lead to limit at best ~ $(8\text{mK})^2$ at z~10 and k~0.05, above most 21-cm signal predictions; With the above improvements this could be reduced to $(\text{few mK})^2$